Measuring the Relative Interface Thickness of Multilayer Polyolefin Films with Atomic Force Microscopy

Rajesh P. Paradkar,[1] Jing Li,[1] Georg Bar,[1] Hoang Pham,[2] Clive Bosnyak,[2]* Jeffrey Weinhold[1]

[1]*Core R&D Analytical Sciences, Dow Chemical Company, Freeport, Texas 77541*
[2]*Plastic R&D, Dow Chemical Company, Freeport, Texas 77541*

Received 13 August 2006; accepted 22 February 2007
DOI 10.1002/app.26550
Published online 16 July 2007 in Wiley InterScience (www.interscience.wiley.com).

ABSTRACT: In any polymer blend system, the nature and thickness of the polymer interface can have a significant influence on the overall performance of the blend. Consequently, it is important to understand the nature of the interactions between the various blend components to effectively design blend combinations with desired end-use properties. However, because of the inherent level of difficulty, the quantitative measurement of the interface thickness in immiscible polymer blends has not been accomplished or reported in the literature. Atomic force microscopy in the tapping mode has been employed to establish a systematic methodology to measure the relative interface thickness of seven types of coextruded multilayer polyolefin films. Criteria have been developed to define profiles of the interface and estimate the interface thickness from these profiles. The effects of tip indentation on the measured value of the interface thickness are also considered. The atomic force microscopy method presented here allows for a direct quantitative estimate of the interface thickness in multilayer polyolefin films, which in turn provides a significantly better understanding of physical properties such as tear in coextruded blown films and the toughness/stiffness balance in injection-molded impact copolymers. © 2007 Wiley Periodicals, Inc. J Appl Polym Sci 106: 1507–1517, 2007

Key words: atomic force microscopy (AFM); blends; interfaces; polyolefins

INTRODUCTION

Since its invention in the early 1980s, atomic force microscopy (AFM) has become an increasingly popular tool for characterizing surfaces and interfaces in many different types of material systems, especially composites. This is because AFM allows the surface and interface properties to be inferred directly. Among the various AFM modes available, nanoindentation and force modulation have almost exclusively been used to estimate the thickness of the interface region. Prado et al.[1] reported an effort to characterize the interface thickness and stiffness using mechanical indentation spectroscopy. Hodzic et al.[2] recently studied the interfacial region in polymer/glass composite materials, using nanoindentation and involving indentations as little as 30 nm deep. They were able to detect the material properties in the transition region between the fiber and matrix and showed that the apparent width of the interface zone was approximately 2–6 μm. However, the calculated elastic moduli of the interface were nearly an order of magnitude larger than those of the bulk matrix. Gao and Mader[3] argued that such a large increase in the modulus above the bulk could not be explained by the presence of the interface alone and attributed it to a boundary effect. It was suggested that a constriction on the development of an indentation plastic zone near the interface increases the resistance to indentation. According to Gao and Mader, to detect the interface width and local mechanical properties with high accuracy, it is preferable to use as small an indenter as possible with exact information about the shape of the indenter tip.[3] VanLandingham et al.[4] studied the interface of a polysulfone–epoxy adhesive system, IM7 graphite fiber in a thermoplastic polyimide matrix, and AS4 carbon fiber in an epoxy matrix.[4] The response of the interface material was different from the response of the bulk epoxy and the bulk polysulfone. These variations in the response were used to estimate the width of the interface, which was found to be approximately 3 μm. Kim et al.[5] studied an E-glass woven fabric reinforced vinyl ester matrix composite and concluded that the nanoindentation test showed an interface approximately 1 μm thick, with large variations between specimens. In addition, these authors noted that nanoindentation was not sensitive enough to identify the effects of different silane agents. However, the nanoscratch test appeared to be sensitive to the type and concentration of the silane agent. The measured thickness of the interface region was found to be 0.8–1.5 μm, depend-

**Present address:* Creative Polymers LLC, Dripping Springs, Texas 78620.
Correspondence to: R. P. Paradkar (rparadkar@dow.com).

ing on the silane agent used. Bogetti et al.[6] performed AFM indentation measurements on an unsized carbon fiber/epoxy system and a coated copper fiber/epoxy system and modeled the actual indentation results, using a three-dimensional finite element model. The finite element model predictions confirmed that the interface region in the unsized fibers was too small (3 nm) in comparison with the physical size of the indentation probe and consequently could not be characterized. In contrast, for the sized fibers, the models suggested that the interface was sufficiently large (50–200 nm) to obtain meaningful results, a prediction that was also validated experimentally.

The other approach based on AFM that is commonly used to study the interface region is the force modulation mode. Force modulation involves using an oscillating cantilever tip that indents into the sample surface. The amplitude of this oscillation is measured as a function of the tip position when the cantilever tip indents cyclically into the sample. Mai et al.[7] probed the interface in glass fiber–epoxy composites, using force modulation, and concluded that the interface was 1–3 μm thick and either ductile or brittle, depending on whether the fiber was sized or unsized, respectively. Munz et al.[8] also used force modulation to characterize the stiffness in a carbon fiber/epoxy composite. Investigations of the cross sections perpendicular to the axis of the carbon fiber were used to determine the thickness of the interface, which was estimated to be between 20 and 80 nm.

In addition to AFM nanoindentation and force modulation, phase imaging in tapping-mode atomic force microscopy (TMAFM) has also been shown to be useful in differentiating between regions of different physical properties, regardless of their topographical nature. The phase angle is defined as the phase lag of the cantilever oscillation with respect to the signal sent to the piezo crystal, driving the cantilever. Its value depends on the balance of attractive/repulsive forces that act on the oscillating cantilever and the energy dissipated in the tapping interaction of the probe and the sample under investigation. The latter, in turn, is related to the viscoelastic properties of the surface. It has been reported that TMAFM routinely achieves a lateral resolution of 10 nm.[3] This resolution limit is primarily imposed by the actual dimension of the tip used to probe the sample. Gao et al.[3] investigated the interface properties of glass-fiber-reinforced polypropylene and epoxy matrix composites, using tapping-mode phase imaging and nanoindentation. This was the only publication that we found in the open literature that employed tapping-mode phase imaging to estimate the interface thickness. It was reported that a good contrast between the fiber, interface, and matrix was observed in the phase images, thereby revealing differences in the material properties of these three regions. This was likely due to a relatively large difference in the hardness between the glass fiber and the matrix, which in turn could aid in determining transitions in the tip response. The interface thickness was estimated to be between less than 100 and approximately 300 nm, depending on the type of sizing agent and matrix material.

In this study, an attempt was made to characterize quantitatively the nature of the interface between two semicrystalline polymers by TMAFM and link this to the calculations of the differences in the solubility parameters.

To overcome the complexity due to the geometry, microlayers of blend components were made to give planar surfaces that mimicked the time–temperature profile that a polymer blend experiences during compounding, but without the mixing element. The blends were designed so that the interaction parameters (interface thickness) between the two phases could be varied by the control of the ethylene content of both the rubber and the matrix. The solubility parameters for the different polymers used in this study were calculated with a procedure similar to the one reported earlier.[9,10] Results from a quantitative analysis of high-resolution TMAFM phase images obtained form a series of polyolefin-based multilayer films are presented to illustrate the approach. Seven blends of isotactic polypropylene with various α-olefin elastomers (rubbers) were used as model systems. Cross-sectional analyses were performed on AFM phase images of these model blends and used to generate profiles of the phase change across (perpendicular to) the interface. Criteria were developed to define the interface and estimate the interface thickness from these cross-sectional phase profiles. The effects of tip indentation on the measured value of the interface thickness were also considered.

EXPERIMENTAL

Materials and microlayer preparation

Some key properties of the commercial resins used for microlayer preparation are shown in Table I. The solubility parameters, given with respect to the value of the polypropylene homopolymer, were determined through an interpolation of the neutron scattering results of Graessley and coworkers.[9,10] The seven multilayer films investigated in this study are summarized in Table II, along with the calculated solubility differences for each polypropylene/rubber pair. The solubility parameter differences [K mol/cm^3] are reported as $(\delta_1 - \delta_2)^2/R$, where δ_1 is the solubility parameter (cal/cm^3)$^{0.5}$ of each component and R is the gas constant. For the films studied, polypropylene homopolymer H110-02N and random

TABLE I
Some Key Properties of the Resins Used for this Study

Polymer	Comonomer	Density (g/cc)	Glass-transition temperature (°C)	Crystallinity (wt %)	MFR or MI	Solubility parameter with respect to polypropylene $[(cal/cm^3)^{0.5}]$
Polypropylene homopolymer H110-02N	—	0.9000	−5	59.3	2 (MFR)	0
Propylene–ethylene copolymer 6D83K (RCP)	3.2 wt % ethylene (C2)	0.9000	—	48.8	1.9 (MFR)	0.0217
Ethylene–octene copolymer Engage 8180 (EO2)	40 wt % octene (C8)	0.8700	−42	12.9	0.5 (MI)	0.4227
Affinity PL-1880 (EO1)	20 wt % octene (C8)	0.9020	<−40	35	1.0 (MI)	0.542
Ethylene–propylene random copolymer (RCP1)	5 wt % ethylene (C2)	0.8870	−18	42.6	2 (MFR)	0.0404
Ethylene–propylene random copolymer (RCP2)	8 wt % ethylene (C2)	0.8745	−21	27.2	2 (MFR)	0.0648
Ethylene–propylene random copolymer (RCP3)	11 wt % ethylene (C2)	0.8650	−27	16.4	2 (MFR)	0.0896
Ethylene–propylene random copolymer (RCP4)	15 wt % ethylene (C2)	0.8577	−30	6.7	2 (MFR)	0.117

MFR, melt flow rate (230°C, 2.16 kg) g/10 min; MI, melt index (190°C, 2.16 kg), g/10 min.

polypropylene copolymer 6D83K were used as the base resins for preparing the microlayers. The multilayer films were of the ABA type (50 : 50 w/w in composition) and had a total of 17 microlayers with a nominal film thickness of approximately 190.5 μm (~7.5 mils). The films were fabricated under the following processing conditions: for the skin layer, extruder zone 1 was 175°C, zone 2 was 210°C, and zone 3 was 235°C for all the films (6D83K and H110-02N-02N based), and for the core layer; extruder zone 1 was 150°C, zone 2 was 210°C, and zone 3 was 235°C for all films except the 6D83K/EO2 multilayer, for which the zone 3 temperature was 220°C. The feed block and die temperatures were 225°C. The glass-transition temperatures and crystallinities (wt %) in the polyolefins were determined by differential scanning calorimetry at 10°C/min. The heats of fusion for polypropylene and polyethylene were taken to be 165 and 290 J/g, respectively.

TABLE II
Multilayer Films and Calculated Solubility Differences for Each Polypropylene/Elastomer Pair

Multilayer material	Solubility difference[b]
6D83K/RCP1[a]	1.75×10^{-4}
6D83K/RCP4	4.54×10^{-3}
6D83K/EO2	8.04×10^{-2}
6D83K/EO1	1.35×10^{-1}
H110-02N/RCP2	2.10×10^{-3}
H110-02N/RCP3	4.01×10^{-3}
H110-02N/RCP4	6.84×10^{-3}
H110-02N/EO1	1.47×10^{-1}

[a] No AFM data were available for this sample.
[b] The data was taken from refs. 9 and 10.

Sample preparation for AFM

A thin strip of the sample film was placed in an embedding mold. The mold was filled with Epofix epoxy (containing 3 wt % hardener) and allowed to cure above room temperature (30–35°C) for 24 h. The cured epoxy block was carefully trimmed with a new razor blade and reduced to a height of approximately 5 mm by careful sawing and sanding of the back (untrimmed) end of the block. The trimmed block was then polished perpendicularly to the machine direction on a Leica Ultracut T microtome (Bannockburn, IL) equipped with an FCS cryosectioning chamber. All the samples were cryogenically polished at −120°C with a special AFM diamond knife (MC 9889, 3 mm, 35° angle) purchased from Diatome (Bienne, Switzerland). During each cut, a 100-nm section was cryofaced. The resulting surfaces were fairly smooth (<200 nm high). The cryogenically polished sample block was then mounted on an AFM sample holder with a quick-curing epoxy. Significant effort was made to ensure that the polished block face was perfectly horizontal.

Sample preparation for transmission electron microscopy (TEM)

Film samples were embedded and cured in Epofix epoxy as described. Once cured, the blocks were trimmed with a razor blade and cryopolished. The cryopolished blocks were stained with vapors of a ruthenium tetraoxide solution for 3 h at room temperature. Sample sections approximately 100 nm thick were cut perpendicularly to the machine direction with a diamond knife on a Leica Ultracut T microtome

equipped with an FCS cryosectioning chamber. The sections were place on formvar-coated copper grids for TEM investigation. Bright-field imaging on a Hitachi H-8100 transmission electron microscope (Pleasanton, CA) was used to obtain the TEM images.

AFM measurements

AFM analysis was performed on the polished sample blocks under ambient conditions with a MultiMode Nanoscope IV scanning probe microscope equipped with a J-scanner (Digital Instruments, Santa Barbara, CA). This scanner allowed imaging of surface areas as large as 190 × 190 μm^2. The microscope was operated in the tapping mode (Veeco, Inc., Santa Barbara, CA), in which the cantilever was oscillated at resonance and the feedback control adjusted for a constant tapping amplitude. Commercial silicon probes with a typical cantilever length of 235 μm were chosen for this work. The nominal spring constants and resonance frequencies of these probes were in the ranges of 37–55 N/m and 164–185 kHz, respectively. The tip radius of curvature, reported by the manufacturer, was less than 10 nm. Because a quantitative measure of the interface thickness was desired and the effects of instrument parameters (e.g., tip shape, scanning rate, and feedback gains) on the measured interface thickness were largely unknown, an empirical approach was adopted. The scan and gain parameters were first optimized with a selected set of samples. All the microlayer samples were subsequently imaged with the same scan and gain settings. Digital height and phase images were acquired simultaneously and are presented as top-view images. To maintain consistency, all the AFM images were acquired from the center of the cross-sectioned films. Before the AFM data were collected, the cantilever was tuned to verify that the phase was zeroed and the resonance frequency was centered with the tip in close proximity to the surface. Except for the image size (1 μm × 1 μm at 512 × 512 pixels or 1 μm × 0.5 μm at 512 × 256 pixels), which was dictated by the available instrument time, the following instrument settings were used throughout this study unless noted otherwise: a scan rate of 0.617 Hz, the free amplitude (A_o) of 3.0 v, and set-point amplitude (A_{sp}) values of 2.5 for the H110-02N series and 2.8 for the 6D83K series.

RESULTS AND DISCUSSION

To image the internal morphology, a film sample has to be polished perpendicularly to the film to create an internal surface. The sample preparation procedure is presented in detail in the Experimental section. Typical AFM phase images for the four samples from the H110-02N series (see Table II) are shown in Figure 1(A-D). AFM phase images for samples from the 6D83K series are presented in Figure 2(A-C). The interface/boundary between the coextruded microlayers is clearly evident in all the phase images. The brighter phase in all the images corresponds to the stiffer, more crystalline H110-02N polypropylene homopolymer or 6D83K polypropylene random copolymer layer, whereas the darker phase represents the corresponding ethylene–octene copolymers (EO1 or EO2) or the ethylene–propylene random copolymers (RCP1–RCP4), depending on the sample composition. For samples H110-02N/EO1 and 6D83K/EO1, the difference in the phase contrast between the layers is not as pronounced as that for the other samples. EO1 is an ethylene–octene copolymer whose density (0.9020 g/cc), that is, crystallinity, is very similar to the density of the polypropylene homopolymer (H110-02N; 0.9000 g/cc) and copolymer (6D83K; 0.9000 g/cc), unlike the ethylene–propylene random copolymers (RCP1–RCP4). It is therefore likely that EO1 is more crystalline and consequently stiffer, resulting in a lower phase contrast than the corresponding ethylene–propylene random copolymers. It has been reported that ethylene–octene copolymers with densities between 0.91 and 0.89 g/cc have a mixed morphology of small lamellae and fringed micellar crystals.[11] Some of these morphological features are evident in the lower resolution images shown in Figure 2 (fringed micellar crystals marked by an arrow).

A few general conclusions can be drawn from a comparison of the AFM phase images of microlayer samples with alternating layers of H110-02N or 6D83K and RCPs containing different amounts of ethylene. It appears that the overall crystallinity of the propylene–ethylene copolymer (darker) phase increases with an increase in the density, that is, a decrease in the ethylene content of the copolymer. In addition, it appears that the interface becomes more diffuse (broad) as the ethylene content in the ethylene propylene random copolymer decreases. This could be attributed to an increase in the thermodynamic interaction between the two layers. Finally, the copolymer layers of the samples in the H110-02N series show well-developed lamellae with a lamellar long axis that are nearly perpendicular to the machine direction, and this is indicative of the molecular orientation.

Although local changes in the chemical and material properties, that is, material property gradients and profiles, have been used[1,3] to estimate the interface thickness in composites and other material systems, the procedure for defining the actual interface from these profiles is still largely subjective. As a result, to maintain consistency in estimating the interface thickness from AFM phase images, a standard procedure had to be developed. It is worth mentioning that this procedure does not necessarily

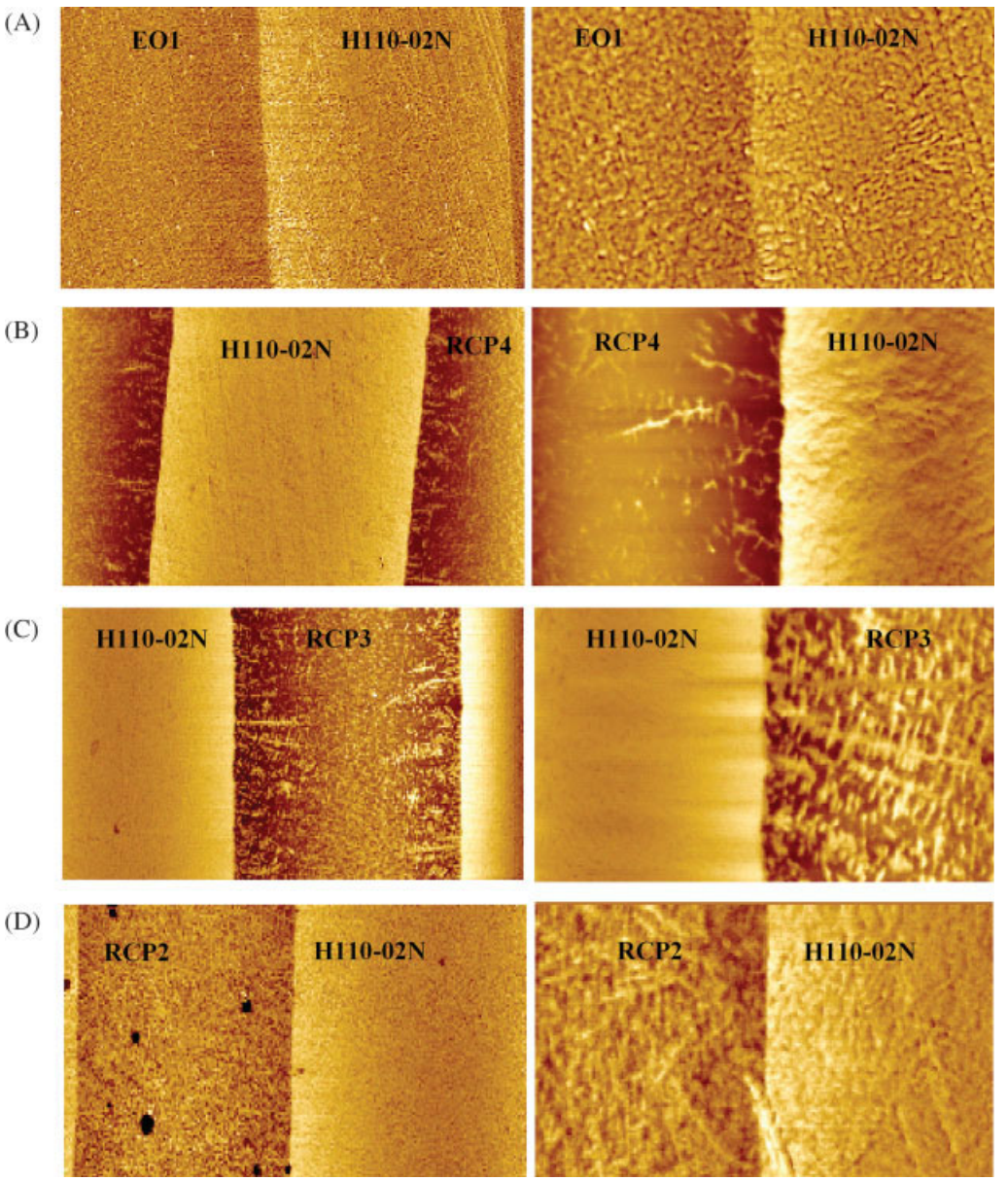

Figure 1 AFM phase images of samples from the H110-02N multilayer series at two magnifications [10 μm × 10 μm (left) and 3 μm × 3 μm (right)]: (A) H110-02N/EO1, (B) H110-02N/RCP4, (C) H110-02N/RCP3, and (D) H110-02N/RCP2. [Color figure can be viewed in the online issue, which is available at www.interscience.wiley.com.]

completely eliminate the subjectivity associated with the data analysis and does not necessarily provide the accuracy to determine the true interface. However, it does improve the precision and reproducibility of measurement by setting criteria for defining the actual interface, that is, defining the baseline and points at which the interface begins and ends. A typical procedure used to estimate the interface thickness from the AFM phase images is briefly outlined, and the measured values of the interface thickness obtained for the different microlayer samples are shown in Table III along with the solubility difference for the polypropylene/rubber pairs. Also included in Table III is an estimation of the interfacial thickness using the formula of Helfand and Tagami[12] with a statistical segment length of 0.62 nm, a reference volume of 50 cm^3/mol, and a temperature of 298 K. The calculated values are in qualitative agreement with the measurements but are generally smaller than the experimental values by a factor of 3–4 or 10–11, depending on whether the elastic layer is a random ethylene–propylene or an ethylene–octene copolymer. A possible reason for the calculations under the prediction of the interfacial thickness is that the polymer pairs do not have a large enough Flory–Huggins interaction parameter to produce the strong segregation that is assumed by the Helfand–Tagami theory.[12]

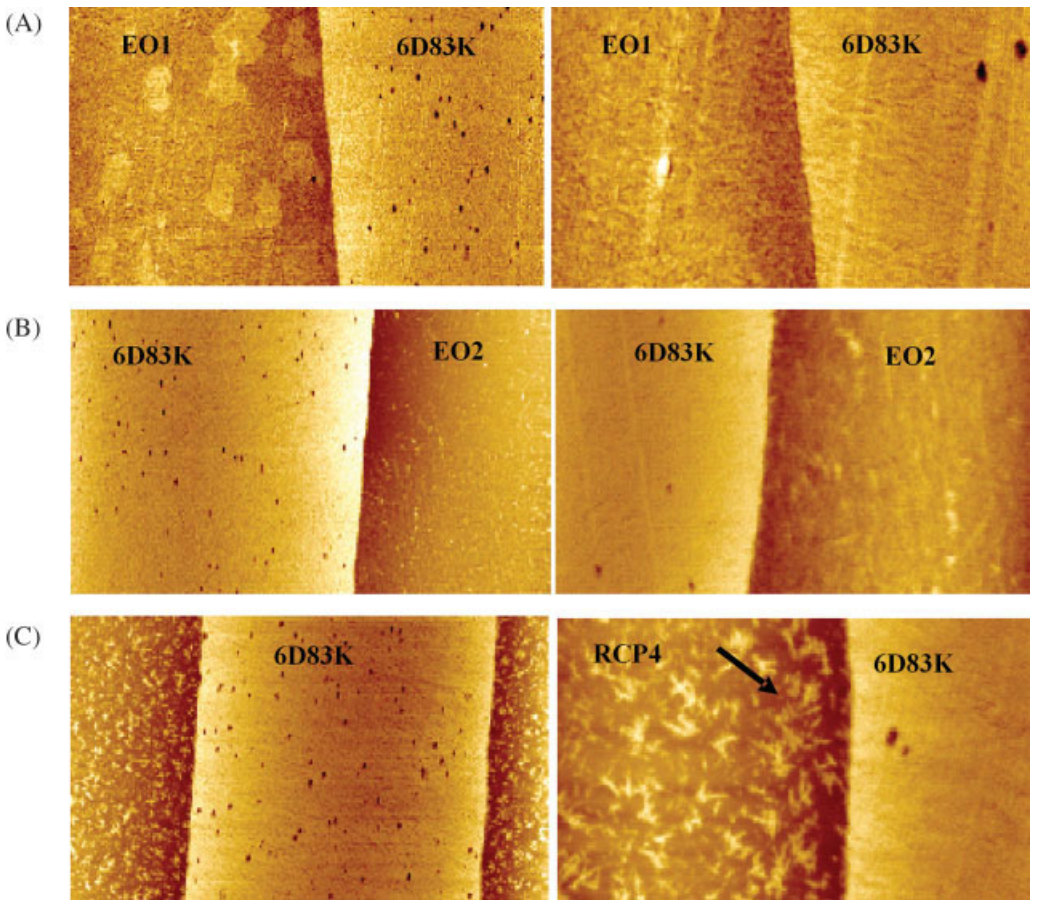

Figure 2 AFM phase images of samples from the 6D83K multilayer series at two magnifications [10 μm × 10 μm (left) and 3 μm × 3 μm (right)]: (A) 6D83K/EO1, (B) 6D83K/EO2, and (C) 6D83K/RCP4. [Color figure can be viewed in the online issue, which is available at www.interscience.wiley.com.]

An artifact-free, high-contrast phase image is the key to obtaining a valid estimate of the interface thickness. A cross-section analysis was performed on the raw phase images (to avoid introducing artifacts due to processing) with the Section Analysis utility available in NanoScope software. The Section Analysis utility generates a profile of the phase change across (perpendicular) the interface. Cross-sectional profiles can be generated along a single line in the phase image, or several line profiles over a defined region can be automatically added together to display an average phase profile. The average phase profile can be used to provide an estimate of the average thickness along the interface and offers several advantages for routine data analysis. Because average profiles are generated by the coaddition of multiple line profiles, they are not as noisy as an individual line profile. This reduces the error involved in defining the baseline and pinpointing the starting and ending points of the interface. In addition, this procedure is much quicker than measuring individual line profiles. A comparison of the interface thickness results for four images from two representative samples obtained with the line and average cross-sectional profile analysis procedures described here are shown in Table IV. Comparable values were obtained with both procedures. For the

TABLE III
Average Interface Thicknesses from AFM Three-Section Analyses and Calculated Solubility Differences for Each Polypropylene/Elastomer Pair

Multilayer polymer film	Solubility difference	Interface thickness (nm)	τ (nm)[a]
6D83K/RCP4	4.54×10^{-3}	77	18
6D83K/EO2	8.04×10^{-2}	42	4
6D83K/EO1	1.35×10^{-1}	38	3
H110-02N/RCP2	2.10×10^{-3}	83	27
H110-02N/RCP3	4.01×10^{-3}	75	20
H110-02N/RCP4	6.84×10^{-3}	58	15
H110-02N/EO1	1.47×10^{-1}	33	3

[a] Estimated interface thickness calculated according to $\tau = 2b/(6\chi)^{1/2}$, where $b = 0.62$ nm is the statistical segment length, $\chi = V_r(\delta_1 - \delta_2)^2/RT$ is the Flory–Huggins interaction parameter estimated from the difference in the solubility parameters, and $V_r = 50$ cm^3/mol is the reference volume.

TABLE IV
Comparison of the Interface Thickness Values Obtained from the Line and Average Cross-Sectional Profile Analysis Procedures

Sample	Measured interface thickness (nm)	
	Line cross-sectional analysis[a]	Average cross-sectional analysis[b]
H110-02N/RCP4 image 3406	53.20 ± 9.23	52.73
H110-02N/RCP4 image 3361	59.98 ± 14.46	60.55
6D83K/RCP4 image 3404	74.86 ± 12.30	78.13
6D83K/RCP4 image 3354	69.09 ± 14.13	72.27

[a] Averages from 45–50 individual line profiles across the entire image. The standard deviations indicate the spread in the interface thickness values from the individual line profile estimates.
[b] In most cases, almost the entire image was averaged with this procedure (maximum of 512 lines × 256 or 512 lines), depending on the image size.

line cross-sectional analysis, at least 45 individual line profiles were measured over the entire phase images. Only the average values and standard deviations for these measurements are reported for brevity.

To determine the interface thickness, a baseline and the starting and ending points for the interface needs to be defined. This is done as follows. The interface thickness is defined as the horizontal distance over which a maximum change in phase (highest slope) is observed. The entire image, in the x direction, is used to define the top and bottom baselines, for the profile. The presence of stiffer domains (crystals) in the EP copolymer layer result in a noisy baseline (see Fig. 3). In such cases, an average baseline is defined to minimize the residuals between the actual phase and the fitted baseline. Next, the top and bottom starting points are defined with the onset method, which is commonly used in calorimetry, and a least-squares tangent is fit between these points. The software automatically calculates the horizontal distance between the starting and ending points, which is the value of the interface thickness. The calculation of the interface thickness, from the AFM image, could potentially be automated with third-party software, and the automated approach may be worth exploring in the future. It is true that the measured interface thickness is a function of the scan size. To get more accurate and statistically valid results, three images, typically with a 1 μm × 1 μm or 1 μm × 0.5 μm scan size, from three different locations along the interface of the film are used to calculate the average interface thickness.

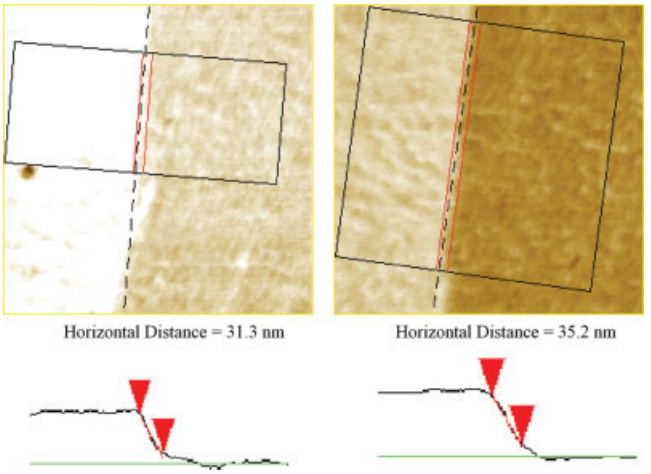

Figure 3 AFM phase images (1 μm × 1 μm) and section analysis results from two images at different locations for sample H110-02N/EO1. [Color figure can be viewed in the online issue, which is available at www.interscience.wiley.com.]

Typical results from the cross-section analysis procedure for all the samples are shown in Figures 4–9. In each case, the results from an analysis of only two sample images are shown. At this point, it is worth mentioning that scanning the free surface of samples from the 6D83K series was more difficult than scanning the free surface of samples from the H110-02N series. This, however, did not appear to be the case when we obtained AFM images of the bulk (cross-sectioned) samples. We speculated that this was likely due to surface migration of the additive(s) or some amorphous (soft) material present in the

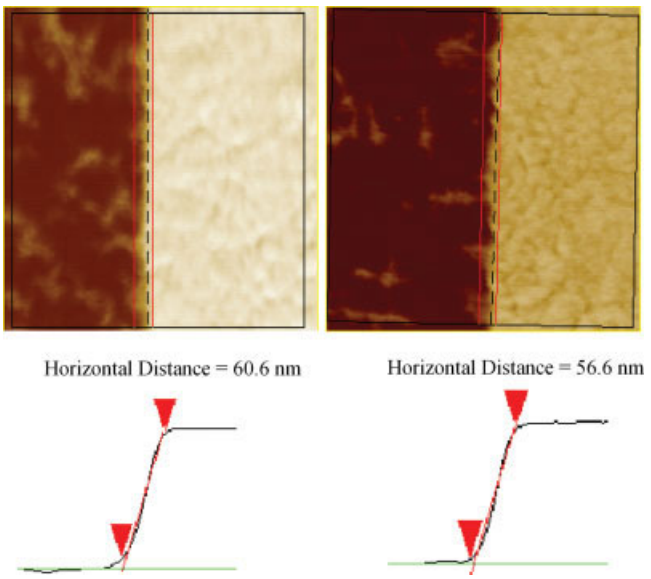

Figure 4 AFM phase images (1 μm × 1 μm) and section analysis results for sample H110-02N/RCP4. [Color figure can be viewed in the online issue, which is available at www.interscience.wiley.com.]

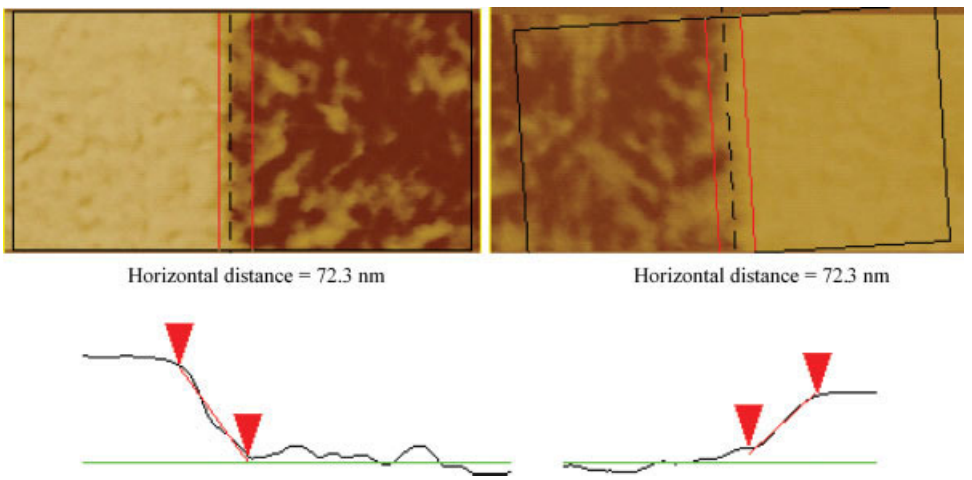

Figure 5 AFM phase images (1 μm × 1 μm) and section analysis results for sample H110-02N/RCP3. [Color figure can be viewed in the online issue, which is available at www.interscience.wiley.com.]

6D83K polypropylene copolymer layer. A plot of the interfacial thickness versus the logarithm of the reciprocal of the solubility parameter difference is shown in Figure 10 and the data used to generate the plot are shown in Table III. Figure 10 suggests that the interfacial thickness increases with a decrease in the solubility parameter difference as expected and is in qualitative agreement with the interfacial thickness calculation proposed in the literature.[12,13]

Finally, to assess the effect of the tip interaction with the sample and its effect on the measured interface thickness, the tapping conditions were varied from light tapping ($A_{sp}/A_o > 0.75$) to moderate tapping ($0.26 < A_{sp}/A_o < 0.74$). This was accomplished by the adjustment of the ratio of A_{sp} to A_o. It was observed that varying the tapping from light to moderate did not significantly affect the measured value of the interface thickness for the samples investigated. As a result, the samples were imaged under light tapping conditions with the largest tapping ratio (lightest tapping) required to obtain good contrast in the phase image. Typically, under these tapping conditions, a higher modulus material appears light in AFM phase images, and a lower modulus material appears dark. Ascertaining the effects of the tip radius of curvature on the measured value of the interface thickness is not straightforward, to say the least. There are two issues that need to be resolved, that is, the diameter of the tip itself and its affect on the resolution and the nonuniformity of the interface, due to the growth of dendritic crystals across the interface, in some regions. On the basis of the experimental results obtained during the course of this study, our best judgment is that the commercial AFM tips used in this study were uniformly fabricated and did not significantly affect the measured value of the interface thickness. In addition, all the interfaces studied are significantly thicker than the physical size of the AFM tip (<10 nm)

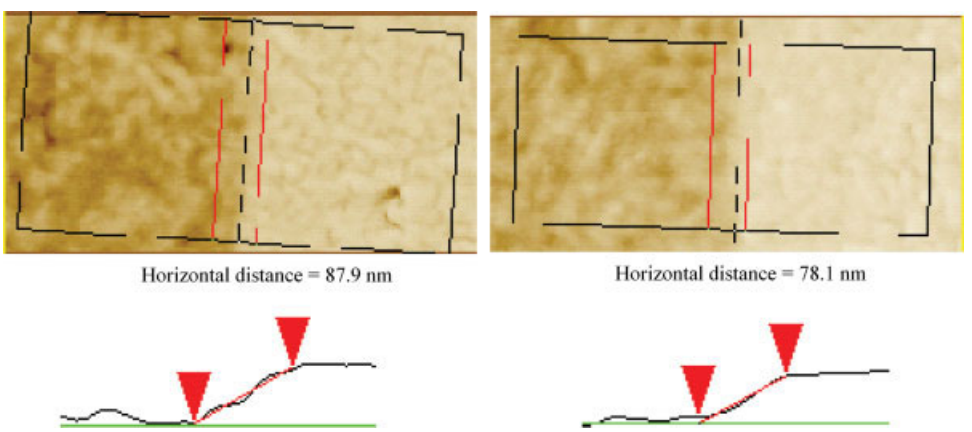

Figure 6 AFM phase images (1 μm × 1 μm) and section analysis results for sample H110-02N/RCP2. [Color figure can be viewed in the online issue, which is available at www.interscience.wiley.com.]

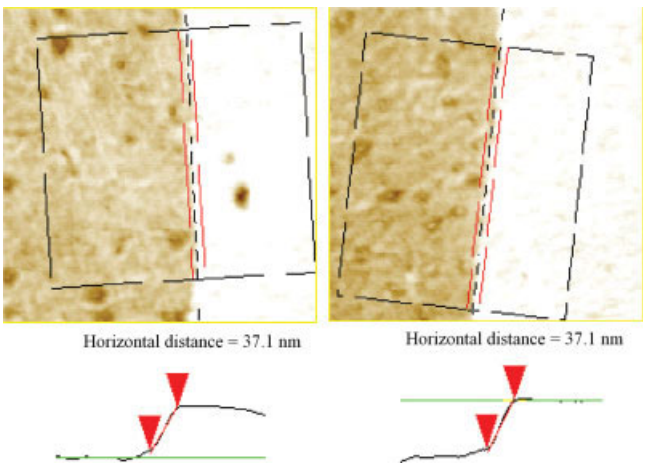

Figure 7 AFM phase images (1 μm × 1 μm) and section analysis results for sample 6D83K/EO1. [Color figure can be viewed in the online issue, which is available at www.interscience.wiley.com.]

and hence well within the measurement sensitivity of the technique

To qualitatively confirm the observations and conclusion based on our AFM approach, TEM images of the interface region were obtained for some representative samples under investigation. Although the physical mechanisms responsible for generating image contrast in AFM and TEM are fundamentally different, a qualitative comparison with an independent technique is highly desirable. Representative TEM images of the interface region of samples H110-02N/EO1, H110-02N/RCP4, and H110-02N/RCP2 are shown in Figures 11–13 and should be compared with the corresponding AFM images

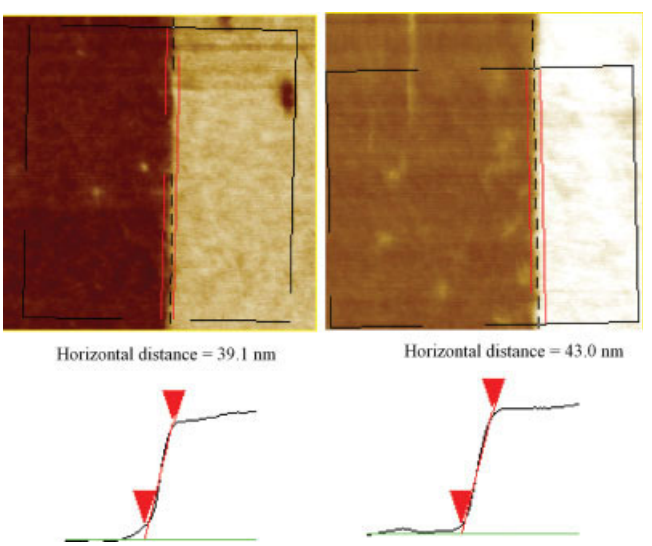

Figure 8 AFM phase images (1 μm × 1 μm) and section analysis results for sample 6D83K/EO2. [Color figure can be viewed in the online issue, which is available at www.interscience.wiley.com.]

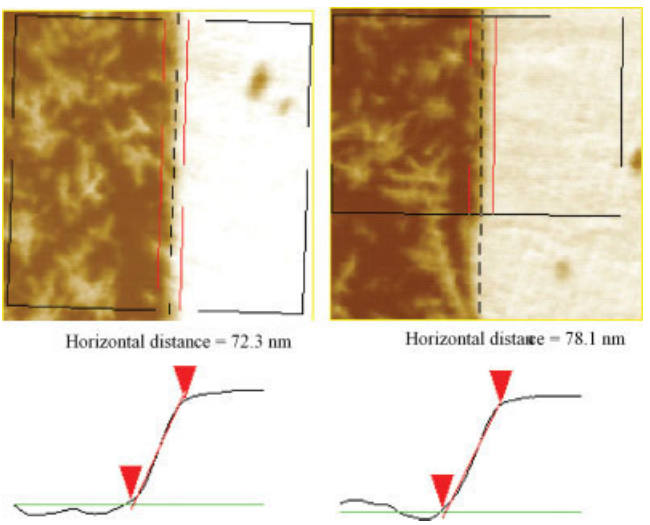

Figure 9 AFM phase images (1 μm × 1 μm) and section analysis results for sample 6D83K/RCP4. [Color figure can be viewed in the online issue, which is available at www.interscience.wiley.com.]

shown in Figure 1(A,B,D), respectively. The TEM images qualitatively agree very well with the AFM observations. The TEM image of H110-02N/RCP4 (Fig. 12) shows that there is very little crystalline lamellar structure revealed within the RCP4 phase, in good agreement with the observation of high, featureless phase contrast observed in the AFM image [Fig. 1(B)]. The interface region between the two layers also appears to be quite sharp in the TEM image. Only short, interpenetrating lamellae (indicated by arrows) associated in both layers can be

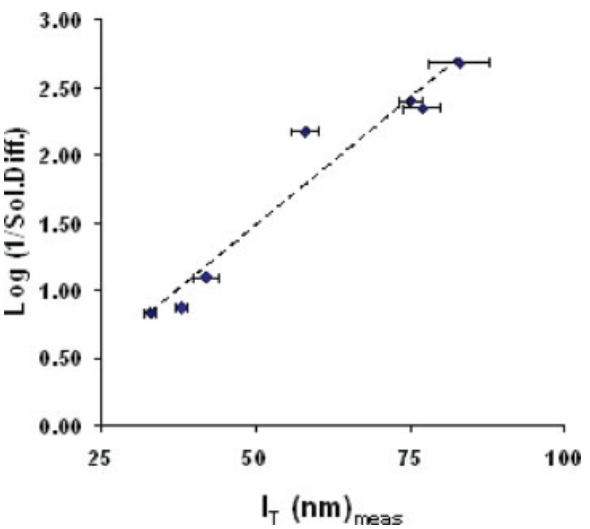

Figure 10 Measured interface thickness as a function of the difference in the solubility parameters for each polypropylene/elastomer pair. The line has been drawn to guide the eye. The error bars show the standard deviation in the measured value of the interface thickness from the analysis of at least three different images.

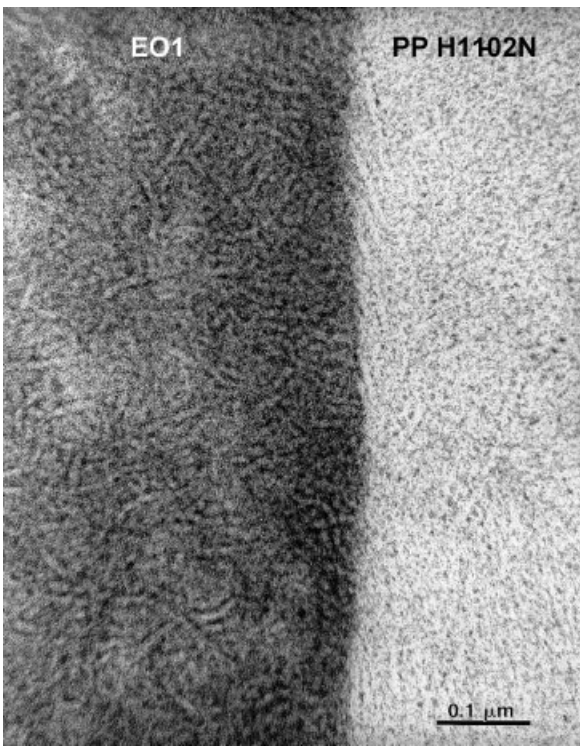

Figure 11 TEM image of sample H110-02N/EO1 [the corresponding AFM image for this sample is shown in Fig. 1(A)].

observed, indicating limited miscibility and compatibility of the two materials. In contrast to sample H110-02N/RCP4, the TEM image of sample H110-02N/EO1 (Fig. 11) shows the presence of crystalline lamellae structures in both phases, H110-02N and EO1. This is also in excellent agreement with the AFM phase image shown in Figure 1(A), which shows a much weaker contrast between the two layers. The TEM image also indicates low miscibility between the H110-02N and EO1 phase because a sharp and linear interfacial boundary can be observed, and lamellae do not penetrate or grow across the layer boundary (Fig. 11). The TEM image of H110-02N/RCP2 (Fig. 13), however, is quite different. Longer and more ordered lamellae can be observed in both the H110-02N and RCP2 layers. The interface boundary between the two layers appears much more diffuse, and within the interfacial region, interpenetrating lamellae are detected that can be associated with both layers (indicated by arrows). Thus, in agreement with the AFM data, the TEM images also indicate higher miscibility between the two phases for the H110-02N/RCP2 sample.

An identical cross-sectional analysis approach, as proposed for AFM, would not necessarily be valid for TEM images because of the different mechanisms underlying AFM and TEM image contrast formation. Therefore, the information content revealed by the two techniques is not identical but complementary. Contrast formation in AFM is due to forces between the tip and sample. Particularly for heterogeneous materials, a strong contrast can be observed in AFM between the material phases if the different sample materials lead to significant force differences. As a result, as the composition varies locally, the tip sample forces will be different, and this will result in phase image contrast variations. On the other hand, being very surface-sensitive, AFM has difficulties visualizing small crystalline structures, such as lamellae, of sectioned surfaces because the sectioning procedure typically introduces some roughness and destruction of these features. Therefore, typically lamellae structures are not visualized in AFM images of sectioned surfaces of semicrystalline materials. To increase contrast between various phases in the TEM images reported here, staining with RuO_4 was required. The incorporation of this heavy metal stain is primarily based on physical absorption and quantitatively is not a well-controlled process. The staining efficiency depends on several factors, but generally phases of lower density stain stronger, such as the amorphous phase of a sample. Visualization of the crystalline structure is therefore possible. TEM, being a transmission method, is also less sensitive to surface defects induced by the sectioning pro-

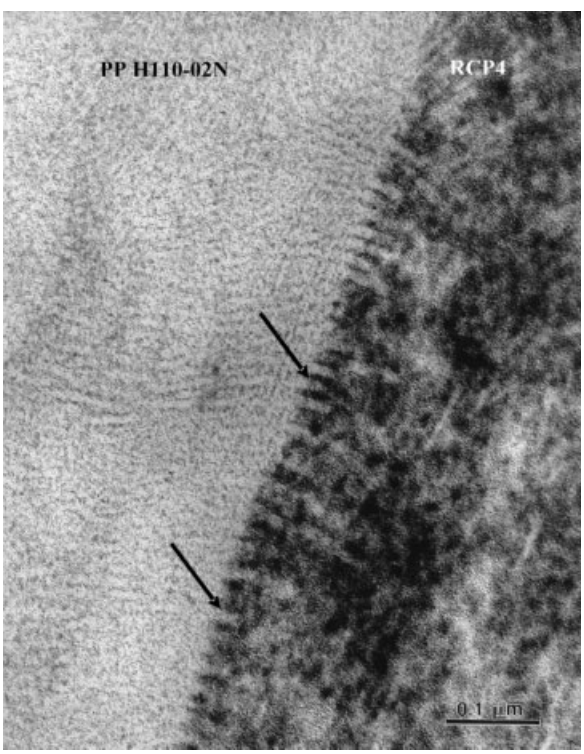

Figure 12 TEM image of H110-02N/RCP4. The arrows indicate short, interpenetrating lamellae oriented perpendicularly to the interface boundary [the corresponding AFM image for this sample is shown in Fig. 1(B)].

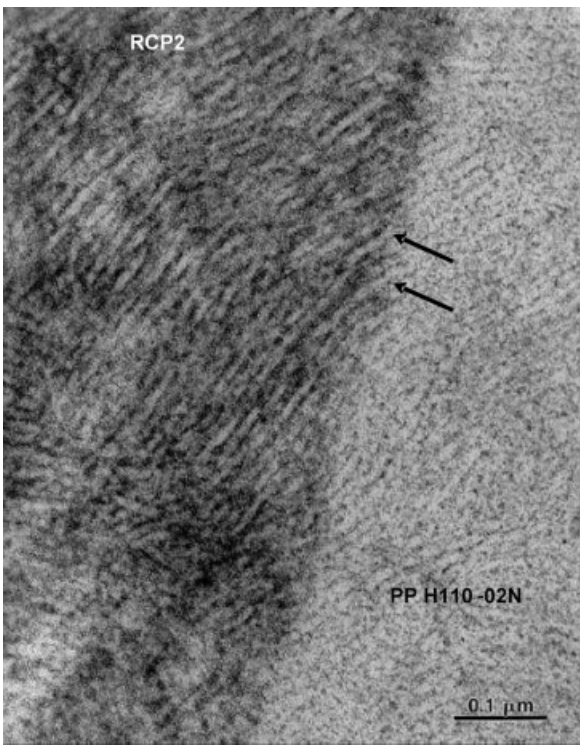

Figure 13 TEM image of H110-02N/RCP2. The arrows indicate long, interpenetrating lamellae associated with both phases [the corresponding AFM image for this sample is shown in Fig. 1(D)].

cedure. On the other hand, local section thickness variations will also result in gray level (contrast) variations observed in TEM. In summary, an identical interpretation of contrast observed in AFM and TEM is not valid, and the methods should be considered complementary.

CONCLUSIONS

We have successfully developed a simple methodology for the routine measurement of the interface thickness in multilayer (17 layer) films, using TMAFM phase imaging. The interface thickness is defined as the horizontal distance over which a maximum change in phase (highest slope) is observed. The method involves acquiring a high-contrast, artifact-free phase image. A profile of the phase change across (perpendicular) the interface is then obtained with the Section Analysis tool available in the NanoScope software. Several line profiles over a defined region are automatically added together to display an average phase profile, thereby providing an estimate of the average thickness along the interface. The entire image in the x direction is used to define the top and bottom baselines for the phase profile. The baseline is defined such that the residuals between the actual phase and the fitted baseline are minimized. Finally, the top and bottom starting points for the interface are defined with the onset method commonly used in calorimetry. A least-squares tangent is fit between these starting and ending points. The horizontal distance between these points is measured as the value of the interface thickness.

In this study, two polypropylene matrices and five different elastomers were employed to examine systematic changes of the interaction parameters between the two phases through the control of the ethylene content of both the rubber and the matrix. The measured interface thickness decreased with an increase in the ethylene comonomer content of the ethylene–octene or propylene–ethylene copolymers. These trends were similar to the ones predicted on the basis of solubility considerations. Although solubility can be used to predict general tends, the amount of the interface cannot be quantified on the basis of solubility considerations alone. The AFM method presented here gives a direct quantitative estimate of the interface thickness, which in turn provides a significantly better understanding of the physical properties, such as tear in coextruded blown films and the toughness/stiffness balance in injection-molded impact copolymers.

The authors thank Steve Werner and Eddy Garcia-Meitin for all their assistance during the course of this project. They acknowledge Harvey Tung, who ran the multilayer coextrusion at Case Western Reserve University, and Eric Baer and Anne Hiltner for their permission to use the equipment. Finally, they thank Dow Chemical Co. for its permission to publish this work.

References

1. Prado, P. J.; Gasper, L.; Fink, G.; Blumich, B.; Herrmann, V.; Unsled, K.; Fuchs, H.-B.; Mohler, H.; Ruhl, M. Macromol Mater Eng 2000, 274, 13.
2. Hodzic, A.; Stachurski, Z. H.; Kim, J. K. Polymer 2000, 41, 6895.
3. Gao, S. L.; Mader, E. Compos A 2002, 33, 559.
4. VanLandingham, M. R.; McKnight, S. H.; Palmese, G. R.; Bogetti, T. A.; Eduljee, R. F.; Gillespie, Jr., J. W. Mater Res Soc Proc 1997, 458, 313.
5. Kim, J. K.; Sham, M. L.; Wu, J. Compos A 2001, 32, 607.
6. Bogetti, T. A.; Wang, T.; VanLandingham, M. R.; Gillespie, J. W., Jr. Compos A 1999, 30, 85.
7. Mai, K.; Mader, E.; Muhle, M. Compos A 1998, 29, 1111.
8. Munz, M.; Strum, H.; Schulz, E.; Hinrichsen, G. Compos A 1998, 29, 1251.
9. Krishnamoorti, R.; Graessley, W. W.; Dee, G. T.; Walsh, D. J.; Jetters, L. J.; Lohse, D. J. Macromolecules 1996, 29, 367.
10. Reichart, G. C.; Graessley, W. W.; Register, R. A.; Lohse, D. J. Macromolecules 1998, 31, 7886.
11. Bensason, S.; Nazarenko, S.; Chum, S.; Hiltner, A.; Baer, E. Polymer 1997, 38, 3913.
12. Helfand, E.; Tagami, Y. J Polym Sci Part B: Polym Lett 1971, 9, 741.
13. Helfand, E.; Tagami, Y. J Chem Phys 1972, 56, 3592.